Acta Mech 231, 1–17 (2020)
https://doi.org/10.1007/s00707-019-02502-y

ORIGINAL PAPER

A. H. Sofiyev · Z. Zerin · N. Kuruoglu

Dynamic behavior of FGM viscoelastic plates resting on elastic foundations

Received: 13 March 2019 / Revised: 31 July 2019 / Published online: 27 September 2019

Abstract The free vibration (FV) and dynamic stability (DS) analysis is presented for functionally graded viscoelastic plates (FGVPs) under compressive load and resting on elastic foundations (EFs). Winkler and Pasternak elastic foundation models are used as elastic foundations. The basic equations of FGVPs interacting with EFs are derived using the concepts of Boltzmann and Volterra. An analytical method for studying the DS and FV of FGVPs interacting with EFs is developed using the integro-differential equations. To solve the current problem, the Galerkin and the Laplace method are used. A technique for the analysis of DS and FV of FGVPs on the EFs is developed. To confirm the proposed formulation, the results are compared with other available solutions. Finally, the influences of EFs, volume fractions and rheological constants on the critical times and frequencies depending on the geometrical characteristics and loading parameters are examined.

1 Introduction

Recently, problems related to the strength, vibration and dynamic stability of plates from composite materials of a new generation, which are the main bearing elements of constructions used in aviation and rocket engineering, mechanical engineering and ships, have been of great interest. As is known, composite materials generally have heterogeneous and viscoelastic properties [1]. The use of new composite materials in engineering practice requires the design and construction of strong, lightweight, reliable structures, the development of mechanical models and mathematical methods that take into account the actual properties of these materials. The general problems of the theory of linear viscoelasticity, that is, the problems of constructing linear and nonlinear hereditary relations between stresses and strains, the reciprocity of such relations, the methods of analytical creep representation and relaxation kernels, and the methods for solving static and dynamic problems are considered in [2–4]. The first attempts to solve DS and FV problems of homogeneous viscoelastic structures are described in refs. [5–8]. These studies and some other works after these publications [9–18] on the viscoelastic behavior of homogeneous structures were considered as the Voigt differential model or the integro-differential Boltzmann–Volterra model using various concepts, constitutive laws and different kernels. An overview of the

A. H. Sofiyev (✉)
Department of Civil Engineering of Engineering Faculty, Suleyman Demirel University, 32260 Isparta, Turkey
E-mail: abdullahavey@sdu.edu.tr
Tel.: 0090 246 211 1195
Fax: 0090 246 237 0859

Z. Zerin
Department of Civil Engineering of Engineering Faculty, Ondokuz Mayis University, Samsun, Turkey

N. Kuruoglu
Department of Civil Engineering of Faculty of Engineering and Architecture, Istanbul Gelisim University, Istanbul, Turkey

solutions of FV and DS problems of homogenous viscoelastic structures (HVSs) in various formulations is given in ref. [19].

A new class of advanced inhomogeneous composite materials was developed, consisting of two or more phases with different material properties and a continuously changing composition distribution, called functionally graded materials (FGMs). One of the first studies on the determination of FGM properties was done by Ostoja-Starzewski et al. [20]. The study [20] presents a method based on micromechanics for treating FGMs and for calculating effective macroscopic properties, which require processing of several length scales: a thin interfacial microstructure, its mesocontinuous representation, the fiber size and the macroscale level. Compared to conventional materials, FGMs have great potential in many areas of technology [21–23]. The mechanical properties of FGMs are often represented in a power-law form [24–27] and in a exponentially graded form [28,29]. FGMs may exhibit time-dependent behavior when used under certain operating conditions. To fully utilize the potential of FGMs, their time-dependent behavior needs to be modeled. A simple model for determining time-dependent behavior is a viscoelasticity model. Currently, some studies have been made on the viscoelasticity theory of functionally graded viscoelastic (FGV) structural elements [30–33]. Based on this fundamental knowledge, some studies have been published on the problems of the static and dynamic behavior of FGV structural elements. Mao et al. [34] examined creep buckling and post-buckling analysis of laminated piezoelectric FGVPs. Zenkour [35] presented an analysis of FGVPs using various theories and Illyushin's approximation method. Shariyat and Nasab [36] investigated the low-speed influence of FGVPs, using the Mori-Tanaka micromechanical model. Barretta et al. [37] solved the problem of torsion of FGV nanobeams using the Laplace method. Yang et al. [38] presented a modified Fourier–Ritz solution for vibration and damping analysis of FGVPs. Deng et al. [39] studied the stability of FGV tubes using the wave propagation method. Li et al. [40] presented nonlocal vibration and stability in the parametric resonance of an axially moving viscoelastic piezoelectric nanoplate. Sofiyev [41,42] solved the dynamic the stability of viscoelastic cylindrical shells made of FGMs and heterogenous orthotropic materials with different initial conditions.

In many engineering applications, since the structural members made of conventional and new composite materials are in contact with various elastic and viscoelastic media, these media may have significant and inevitable effects on the FV and DS behavior of structural components. The various foundation models and their effects on the behavior of structural elements are found in the fundamental works [43–45]. The viscoelastic structural elements in contact with various elastic foundations are widely used in modern technologies and represent serious technical problems in the design. The solution of such problems motivates many researchers to examine the behavior of FGV structures in contact with various types of EFs. Zenkour et al. [46,47] presented bending analysis of FGV beams and plates resting on the PEF. Shariyat and Alipour [48] analyzed FV and damping effect of FGV plates with variable thickness on the PEF. Hosseini et al. [49] studied the forced response of a viscoelastic piezoelectric beam on the nonlinear EFs under external harmonic excitation. Sobhy and Zenkour [50] investigated the influence of a magnetic field on the thermomechanical buckling and vibration of viscoelastic sandwich nanobeams with reinforced CNT face sheets on the viscoelastic substrate. Liu et al. [51] investigated the vibration of FGV magneto-electro-porous nanobeams on the visco-PEF. Deniz et al. [52] studied elastic foundation effects on the frequency parameter of FGM shells in the framework of SDT. Haciyev et al. [53] studied vibration inhomogeneous with spatial coordinate's elastic plates on the inhomogeneous viscoelastic foundation.

A wide literature review shows that dynamic stability and vibration of FGVPs on EFs have not been sufficiently studied so far. The purpose of this study is to build models and conduct studies on dynamic stability and vibration of FGVPs resting on WEF and PEF. The mechanical behavior of the plate material is described by the viscoelastic body model, which is based on the Boltzmann–Volterra principle. The relationship between stress and strain obeys the linear Volterra–Feucht equation. To solve the current problem Galerkin and Laplace methods are used. The practical value of the study is that the developed models and methods allow implementing a qualitatively new approach when designing FGVPs interacting with EFs, reducing the time spent on natural and numerical experiments, and in some cases replacing them with analytical estimates.

2 Modeling of the problem

The schematic diagram of the FGVP subjected to the compressive load P and resting on EFs with mean length a, width b and thickness h is presented in Fig. 1. The referred coordinate system $(Ox_1x_2x_3)$ is in the reference surface of the FGVP and its origin is located at the left corner of the rectangular plate. The displacements U_1, U_2 and U_3 are in the direction of the axes x_1, x_2 and x_3, respectively. Let Φ be the airy stress function for

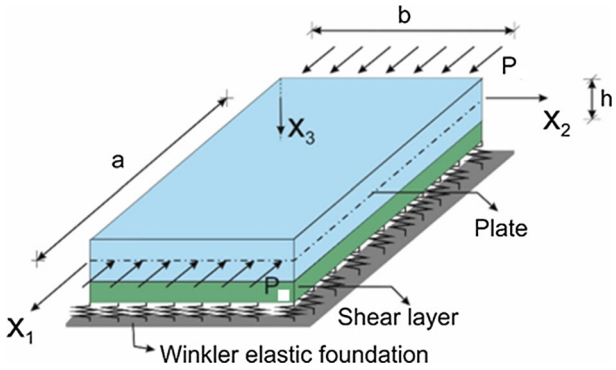

Fig. 1 FGVP on the Pasternak elastic foundation with coordinate convention

the stress resultants defined by $(n_{11}, n_{22}, n_{12}) = \left(h\frac{\partial^2\Phi}{\partial x_2^2}, -h\frac{\partial^2\Phi}{\partial x_1 \partial x_2}, h\frac{\partial^2\Phi}{\partial x_1^2}\right)$. It is also assumed that the normal stresses acting on the reference surface are negligible compared to other force components.

The effective material properties P_f of the FGVPs are defined as [22]

$$P_f = P_0\left(P_{-1}T^{-1} + 1 + TP_1 + T^2P_2 + T^3P_3\right), \tag{1}$$

where $P_i, i = -1, 0, \ldots, 3$ are the coefficients of temperature T(K).

The effective properties of FGMs based on the Voight model are expressed as follows:

$$\bar{P} = \sum_{i=1} P_i V_i, \tag{2}$$

where $\bar{P}$ is the generic material property, P_1 and P_2 are the properties of ceramic and metal, respectively, and the volume fraction of the ceramic (or metal) phase is defined with the inverse quadratic relation

$$V(x_3) = 1 - \left(\frac{1}{2} - \frac{x_3}{h}\right)^2 \tag{3}$$

It should be emphasized that if the volume fraction of the ceramic phase is $V(x_3)$, the volume fraction of the metal phase becomes $1 - V(x_3)$ or vice versa [27].

Based on the aforementioned rule of mixture, the effective material properties of FGMs are written as a function of the thickness coordinate [22–27]:

(a) If the lower surface is ceramic-rich, the effective material properties of FGMs are expressed as

$$E_f = (E_1 - E_2)V(x_3) + E_2, \quad \nu_f = (\nu_1 - \nu_2)V(x_3) + \nu_2, \quad \rho_f = (\rho_1 - \rho_2)V(x_3) + \rho_2; \tag{4a}$$

(b) If the lower surface is metal-rich, the effective material properties of FGMs are expressed as

$$E_f = (E_2 - E_1)V(x_3) + E_1, \quad \nu_f = (\nu_2 - \nu_1)V(x_3) + \nu_1, \quad \rho_f = (\rho_2 - \rho_1)V(x_3) + \rho_1, \tag{4b}$$

where E_1, E_2, ν_1, ν_2 and ρ_1, ρ_2 are elasticity modulus, Poisson's ratio and density of ceramic and metal surfaces of FGMs, respectively. Additional information on the FGM profiles is provided [20–29].

Some researchers used an exponential function to describe the effective material properties of FGMs as follows [28,29]:

(a) If the lower surface is ceramic-rich:

$$E_f = E_2 e^{\left(\frac{1}{2}+\frac{x_3}{h}\right)\ln\left(\frac{E_1}{E_2}\right)}, \quad \nu_f = \nu_2 e^{\left(\frac{1}{2}+\frac{x_3}{h}\right)\ln\left(\frac{\nu_1}{\nu_2}\right)}, \quad \rho_f = \rho_2 e^{\left(\frac{1}{2}+\frac{x_3}{h}\right)\ln\left(\frac{\rho_1}{\rho_2}\right)}. \tag{5a}$$

(b) If the lower surface is metal-rich:

$$E_f = E_1 e^{\left(\frac{1}{2}+\frac{x_3}{h}\right)\ln\left(\frac{E_2}{E_1}\right)}, \quad \nu_f = \nu_1 e^{\left(\frac{1}{2}+\frac{x_3}{h}\right)\ln\left(\frac{\nu_2}{\nu_1}\right)}, \quad \rho_f = \rho_1 e^{\left(\frac{1}{2}+\frac{x_3}{h}\right)\ln\left(\frac{\rho_2}{\rho_1}\right)}. \tag{5b}$$

In the analysis section, it will be indicated which of the expressions (4a), (4b), (5a) and (5b) is used in tables or comments in order to understand the type of FGM.

2.1 The governing equations

The dynamic stability and compatibility equations of FGVPs resting on the PEF are [1,41,53]:

$$\frac{\partial^2 m_{11}}{\partial x_1^2}+2\frac{\partial^2 m_{12}}{\partial x_1 \partial x_2}+\frac{\partial^2 m_{22}}{\partial x_2^2}-P\frac{\partial^2 U_3}{\partial x_1^2}+K(U_3)=\bar{\rho}_f\frac{\partial^2 U_3}{\partial \tau^2}, \tag{6}$$

$$\frac{\partial^2 e_{11}}{\partial x_2^2}+\frac{\partial^2 e_{22}}{\partial x_1^2}-\frac{\partial^2 \gamma_{12}}{\partial x_1 \partial x_2}=0, \tag{7}$$

where $m_{ij}(i=1,2)$ are the moment components, τ is the time, $e_{11}, e_{22}, \gamma_{12}$ are the strains in the reference surface, and $\bar{\rho}_f=\int\limits_{-h/2}^{h/2}\rho_f \mathrm{d}x_3$. Here $K(U_3)$ is the differential operator that defines the effect of the PEF on the plates and is given in the following form:

$$K(U_3)=-k_w U_3+k_p\left(\frac{\partial^2 U_3}{\partial x_1^2}+\frac{\partial^2 U_3}{\partial x_2^2}\right) \tag{8}$$

in which k_w (in N/m^3) is the modulus of the WEF and k_P (in N/m) is the shear modulus of the PEF. When $k_P=0$, the PEF is transformed into the WEF [43–45].

In this study, it is assumed that the Kirchhoff–Love hypotheses are valid and the protection of isotropy is given throughout the deformation process. The relationship between stresses and strains for FGVPs using the Boltzmann–Volterra principle takes the form [1,42]

$$\sigma_1=\frac{E_f}{1-\nu_f^2}(1-R^*)\left(\varepsilon_1+\nu_f\varepsilon_2\right),\ \sigma_2=\frac{E_f}{1-\nu_f^2}(1-R^*)\left(\varepsilon_2+\nu_f\varepsilon_1\right),$$
$$\sigma_{12}=\frac{E_f}{2(1+\nu_f)}(1-R^*)\gamma_{12}, \tag{9}$$

and R^* is the integral operator with the relaxation kernel $R(\tau-t)$ [1,3,4]:

$$R^*\left[\Theta(\tau)\right]=\int\limits_0^\tau R(\tau-t)\Theta(t)\mathrm{d}t \tag{10}$$

At $\tau\to 0$, the resistance of the FGVPs tends to that of ideal FG elastic plates.

The force and moment components are found from the following integrals [1,22]:

$$\left(n_{ij},m_{ij}\right)=\int\limits_{-h/2}^{h/2}\sigma_{ij}\left[1,x_3\right]\mathrm{d}x_3,\qquad (i,j)=(1,2). \tag{11}$$

Substituting Eq. (9) into the integral (11) and resulting relations into Eqs. (6) and (7), and performing some manipulation, the system of integro-differential equations for the FGVPs resting on the PEF is obtained:

$$\left(L_{11}\Phi+L_{12}U_3\right)\left(1-R^*\right)+L_{13}U_3=0,$$
$$\left(L_{21}\Phi+L_{22}U_3\right)\left(1-R^*\right)=0, \tag{12}$$

where $L_{ij}(i,j=1,2,3)$ are differential operators, which are given in Appendix A.

3 Solution of governing equations

Let the edges of the FGVP be simply supported; with the use of the Galerkin method, the solution of Eq. (12), satisfying the boundary conditions of the problem, will be sought in the form [1,53]:

$$U_3 = f_1(\tau)\sin(\lambda_1 x_1)\cos(\lambda_2 x_2), \quad \Phi = \Phi_1(\tau)\sin(\lambda_1 x_1)\cos(\lambda_2 x_2), \tag{13}$$

where $f_1(\tau)$ and $\Phi_1(\tau)$ are time dependent unknown functions, $\lambda_1 = \frac{m\pi}{a}$ and $\lambda_2 = \frac{n\pi}{b}$ in which m and n are half-wave numbers in the longitudinal and transverse directions.

Substituting (13) into the system of equations (12), performing the Galerkin procedure and removing $\Phi_1(\tau)$ from the system, the following integro-differential equation is obtained:

$$\bar{\rho}_f \frac{d^2 f_1(\tau)}{d\tau^2} + \left[D\left(1 - R^*\right) + k_w + k_p\left(\lambda_1^2 + \lambda_2^2\right) - P\lambda_1^2\right] f_1(\tau) = 0, \tag{14}$$

where

$$D = u_3\lambda_1^4 + 2\left(u_4 + u_6\right)\lambda_1^2\lambda_2^2 + u_3\lambda_2^4 - \frac{u_2\lambda_1^4 + 2\left(u_1 - u_5\right)\lambda_1^2\lambda_2^2 + u_2\lambda_2^4}{v_1\lambda_1^4 + \left(2v_2 + v_5\right)\lambda_1^2\lambda_2^2 + v_1\lambda_2^4} \times \left[v_4\lambda_1^4 + \left(2v_3 - v_6\right)\lambda_1^2\lambda_2^2 + v_4\lambda_2^4\right]. \tag{15}$$

To solve Eq. (14), the initial conditions are defined as follows:

$$f_1(0) = f_{10}, \quad f_1'(0) \neq f_{11}, \quad f_1''(0) = 0, \text{ as } \tau = 0. \tag{16}$$

The Laplace transform is a powerful method for solving linear problems in mathematical physics, including problems of the linear theory of viscoelasticity. To solve Eq. (14), we will use this method. Let's convert Eq. (14) with the Laplace transform as follows:

$$F_1(\xi) = \frac{(\xi + \alpha)\left(\xi f_{10} + f_{11}\right)}{\xi^3 + \alpha\xi^2 + \vartheta\left(1 - \upsilon\right)\xi - \vartheta\alpha\left(\upsilon - k_{wp}\right)}, \tag{17}$$

where $R(\tau - t) = \alpha e^{-\alpha(\tau - t)} (0 < \alpha < 1)$, in which α denotes a viscoelasticity parameter, ξ is the variable in image, $F_1(\xi)$ is image of the original function $f_1(\tau)$ and the following symbols are used:

$$F_1(\xi) = \int_0^\infty f_1(\tau) e^{-\xi\tau} d\tau, \upsilon = \frac{P}{P_{cr}^{wp}}, k_{wp} = \frac{k_w + k_p\left(\lambda_1^2 + \lambda_2^2\right)}{\lambda_1^2 P_{cr}^{wp}},$$
$$\vartheta = \frac{D + k_w + k_p\left(\lambda_1^2 + \lambda_2^2\right)}{\bar{\rho}_f} = \omega_{wp}^2, \tag{18}$$

in which ω_{wp} is the frequency for FG elastic plates on the PEF.

To facilitate separation into simple fractions, Eq. (17) is rewritten as

$$F_1(\xi_1) = \frac{(1 + \xi_1)\left(\tilde{f}_{10}\xi_1 + \tilde{f}_{11}\right)}{\xi_1^3 + \xi_1^2 + \vartheta_1(1 - \upsilon)\xi_1 - \vartheta_1(\upsilon - k_{wp})}, \tag{19}$$

where

$$\xi_1 = \frac{\xi}{\alpha}, \quad \tilde{f}_{10} = \frac{f_{10}}{\alpha}, \quad \tilde{f}_{11} = \frac{f_{11}}{\alpha^2}, \quad \vartheta_1 = \frac{\vartheta}{\alpha^2}. \tag{20}$$

Due to the fact that $\upsilon - k_{wp} > 0$ and $\vartheta_1 >> 1$ [1,42], one of the positive roots that convert the denominator of Eq. (19) to zero is η_1^{wp}, the other two roots are as follows:

$$\eta_{2,3}^{wp} = -\frac{1 + \eta_1^{wp}}{2} \pm i b_{wp}, \tag{21}$$

where

$$\eta_1^{wp}=\frac{\vartheta_1(\upsilon-k_{wp})}{\vartheta_1(1-\upsilon)+\eta_1^{wp}(1+\eta_1^{wp})},\ b_{wp}=\sqrt{\vartheta_{2wp}-\frac{\left(1-\eta_1^{wp}\right)^2}{4}}, \tag{22}$$

in which $\vartheta_{2wp}=\left(\eta_1^{wp}\right)^2+\vartheta_1(1-\upsilon)$ and $\vartheta_{2wp}-\frac{\left(1-\eta_1^{wp}\right)^2}{4}>0$. The expression (19) is easily converted to the following form:

$$\begin{aligned}F_1(\xi_2)=\tilde{f}_{10}&\left[\frac{x(y_2-y_1)+x^2-y_1y_2}{x^2+b_{wp}^2}\frac{1}{\xi_2-x}+\right.\\&\left.+\frac{b_{wp}^2-x(y_2-y_1)+y_1y_2}{x^2+b_{wp}^2}\frac{\xi_2}{\xi_2^2+b_{wp}^2}+\frac{xb_{wp}^2+b_{wp}^2(y_2-y_1)+xy_1y_2}{x^2+b_{wp}^2}\frac{1}{\xi_2^2+b_{wp}^2}\right]\\&+\tilde{f}_{11}\left[\frac{x+y_2}{x^2+b_{wp}^2}\cdot\frac{1}{\xi_2-x}-\frac{x+y_2}{x^2+b_{wp}^2}\cdot\frac{\xi_2}{\xi_2^2+b_{wp}^2}+\frac{b_{wp}^2-xy_2}{b_{wp}(x^2+b_{wp}^2)}\cdot\frac{b_{wp}}{\xi_2^2+b_{wp}^2}\right],\end{aligned} \tag{23}$$

where

$$y_1=\frac{1+\eta_1^{wp}}{2},\quad y_2=\frac{1-\eta_1^{wp}}{2},\quad x=\frac{1+3\eta_1^{wp}}{2},\quad \xi_2=\xi_1+\frac{1+\eta_1^{wp}}{2}. \tag{24}$$

Equation (23) takes the following form after the inverse Laplace transformation:

$$f_1(\tau_1)=(C_1+C_4)e^{\eta_1^{wp}\tau_1}+\left[(C_2+C_5)\cos\left(b_{wp}\tau_1\right)+(C_3+C_6)\sin\left(b_{wp}\tau_1\right)\right]e^{-\frac{1+\eta_1^{wp}}{2}\tau_1}, \tag{25}$$

where

$$\begin{aligned}&C_1=\frac{x(y_2-y_1)+x^2-y_1y_2}{x^2+b_{wp}^2}\tilde{f}_{10},\quad C_2=\frac{b_{wp}^2-x(y_2-y_1)+y_1y_2}{x^2+b_{wp}^2}\tilde{f}_{10},\\&C_3=\frac{xb_{wp}^2+b_{wp}^2(y_2-y_1)+xy_1y_2}{x^2+b_{wp}^2}\cdot\frac{\tilde{f}_{10}}{b_{wp}},\quad C_4=-C_5=\frac{x+y_2}{x^2+b_{wp}^2}\tilde{f}_{11},\\&C_6=\frac{b_{wp}^2-xy_2}{x^2+b_{wp}^2}\frac{\tilde{f}_{11}}{b_{wp}},\quad \tau_1=\alpha\tau.\end{aligned} \tag{26}$$

For the initial condition A (ICA): $f_1(0)=f_{10}$, $f_1'(0)=0$, since $\vartheta_{2wp}>>1$, the inequality $C_3<<C_2$ is satisfied and the expression (25) takes the form:

$$f_{11}(\tau_1)=C_1e^{\eta_1^{wp}\tau_1}+C_2e^{-\frac{1+\eta_1^{wp}}{2}\tau_1}. \tag{27}$$

The expression for the critical time is found from the condition $f_{11}'(\tau_1)=0$ as

$$\tau_{11wp}^{cr}=\frac{2}{1+3\eta_1^{wp}}\ln\left(\frac{1+\eta_1^{wp}}{2\eta_1^{wp}}\frac{C_2}{C_1}\right). \tag{28}$$

For the initial condition B (ICB): $f_1(0)=0$, $f_1'(0)=f_{11}$, since $\vartheta_{2wp}>>1$, the inequality $C_5<<C_6$ is satisfied and the expression (25) takes the form

$$f_{12}(\tau_1)=C_4e^{\eta_1^{wp}\tau_1}+C_6e^{-\frac{1+\eta_1^{wp}}{2}\tau_1}. \tag{29}$$

The critical time is obtained from the following expression:

$$\tau_{12wp}^{cr}=\frac{2}{1+3\eta_1^{wp}}\ln\left(\frac{1+\eta_1^{wp}}{2\eta_1^{wp}}\frac{C_6}{C_4}\right). \tag{30}$$

The magnitudes of CTs for FGVPs resting on the PEF can be found using Eqs. (28) and (30) for ICA and ICB, respectively.

In particular, for $\upsilon - k_{wp} = 0$, from Eq. (25), the equation for the FV is obtained as:

$$f_2(\tau_1) = \left[(C_2 + C_5)\cos\left(b_{wp}\tau_1\right) + (C_3 + C_6)\sin\left(b_{wp}\tau_1\right)\right] e^{-\frac{1+\eta_1^{wp}}{2}\tau_1}. \tag{31}$$

We can easily convert the equation of the FV for the FGVPs resting on the PEF into the following form:

$$f_2(\tau_1) = a_{wp} e^{-\frac{1+\eta_1^{wp}}{2}\tau_1}\cos(b_{wp}\tau_1 - \gamma), \tag{32}$$

where

$$a_{wp} = \sqrt{(C_2 + C_5)^2 + (C_3 + C_6)^2}, \quad \gamma = \arctan\frac{C_3 + C_6}{C_2 + C_5}. \tag{33}$$

From Eqs. (32) or (33), the frequency of the FV for the FGVPs resting on the PEF is obtained as:

$$\omega_{wp}^{FGVCS} = \sqrt{\vartheta_{2wp}}. \tag{34}$$

When $k_w = 0$ in Eqs. (27)–(34), the appropriate equations for FGVPs on the WEF are obtained. In the case of $k_w = k_p = 0$, from Eqs. (27)–(34), the appropriate equations for unconstrained FGVPs are obtained.

4 Results and discussion

4.1 Comparative studies

To confirm the validity of the present study, we compared our results with those of Matyash [54], who solved the free vibration of homogeneous isotropic viscoelastic shells (HIVSs) without EFs, and obtained the formula for the amplitude with the ICA, i.e., with $f_1(0) = f_{10}$, $f_1'(0) = 0$:

$$\widehat{f}(\tau) = \widehat{a}\, e^{\frac{-\sqrt{\widehat{D}}\,\widehat{\varepsilon}\,\widehat{A}}{2}\tau}\cos\left[\sqrt{\widehat{D}}\left(\frac{\widehat{\varepsilon}\,\widehat{B}-2}{2}\right)\tau - \widehat{\phi}\right], \tag{35}$$

where the following definitions apply:

$$\widehat{a} = f_{10}\sqrt{\frac{4\widehat{n}^2}{\left(\widehat{\varepsilon}\,\widehat{B}-2\right)^2\widehat{D}} + 1}, \quad \widehat{n} = \frac{\widehat{\varepsilon}\,\widehat{A}\sqrt{\widehat{D}}}{2}, \quad \widehat{\phi} = \arctan\frac{2\,\widehat{n}}{\left(\widehat{\varepsilon}\,\widehat{B}-2\right)\sqrt{\widehat{D}}},$$
$$\widehat{A} = \frac{\sqrt{\widehat{D}}}{\widehat{D}+\alpha^2}, \quad \widehat{B} = \frac{1}{\widehat{D}+\alpha^2}, \tag{36}$$

in which $\widehat{D}$ is the parameter for a HIVS, similar to the parameter D in the present study. Here L is the length and R is the radius of the HIVS.

At $C_3 = C_6 = 0$; $k_w = k_p = 0$; $V_2 = 0$, $\tau_1 = \tau\alpha$, Eq. (32) in the current study and Eq. (35) obtained by Matyash [54] are used in the calculations using the following physical and geometrical data:

$$L = a,\ b = \pi R,\ a/h = 50,\ a/b = 2,\ E_2 = 2.0104\times10^{11}\ (\text{Pa}),\ \rho_2 = 8.166\times10^3\ \text{kg/m}^3,$$
$$\nu_2 = 0.3262,\ f_{10} = 0.001,\ \alpha = 0.06,\ \widehat{\varepsilon} = 0.06.$$

As can be seen from Figs. 2a, b, the amplitude for the free vibration on the unconstrained viscoelastic plate in our study is consistent with the results of Matyash [54].

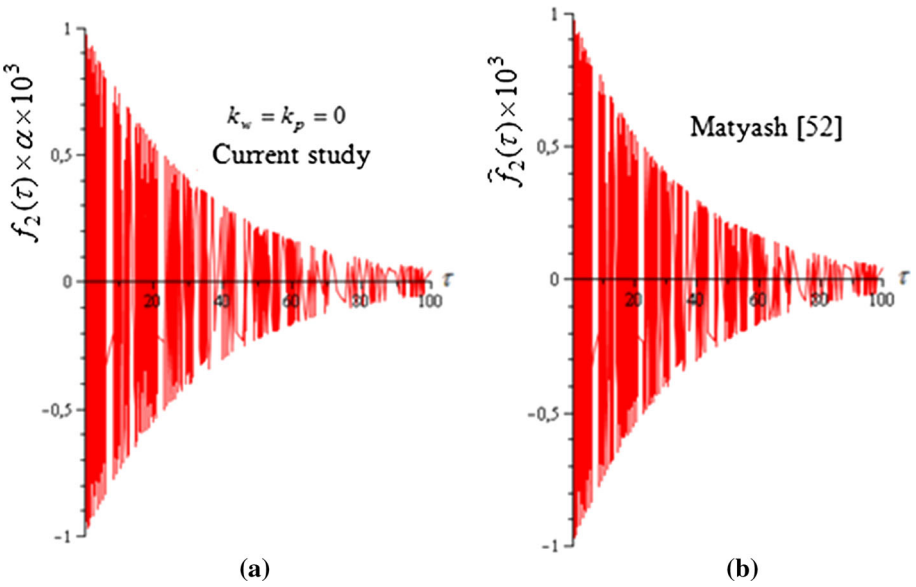

(a) **(b)**

Fig. 2 Comparison of the amplitude of FV for the unconstrained HIVP versus the τ, **a** in the current study and **b** in study of Matyash [54]

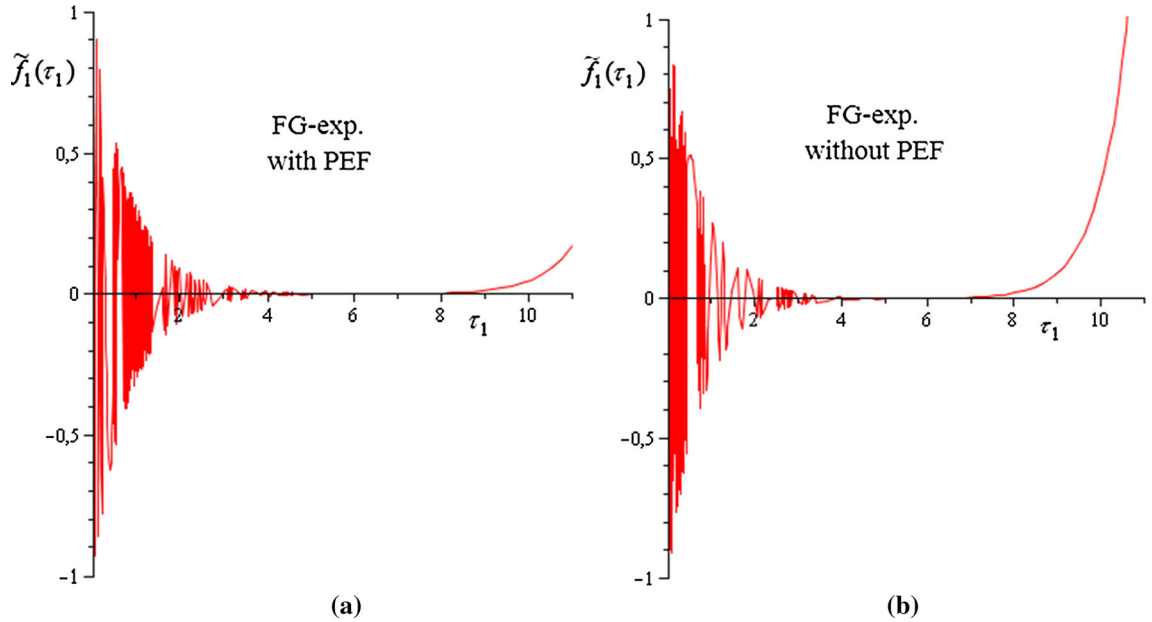

(a) **(b)**

Fig. 3 Change of $\tilde{f}_1(\tau_1)$ for FG-exponential VPs **a** with PEF and **b** without PEF against the τ_1 for the ICA ($f_1(0) = f_{10}$, $f_1'(0) = 0$)

4.2 DS and FV analysis of FGVPs with and without EFs

In this subsection, some analyses have been made for time-dependent changes of amplitudes for DS and FV of FG-exponential and FG-inverse quadratic VPs resting on the PEF, using the formulas (27)–(30). The material properties of the FGM consist of a mixture of silicon nitrite (Si_3N_4) and stainless steel (SUS304) obtained using the expression (1) for $T = 300\,(K)$, as follows [21]:

$$E_1 = 2.07788 \times 10^{11}\,(\text{Pa}), \quad E_2 = 3.22271 \times 10^{11}\,(\text{Pa}), \quad \nu_1 = 0.317756, \quad \nu_2 = 0.24,$$
$$\rho_1 = 8166\ \text{kg/m}^3, \quad \rho_2 = 2370\ \text{kg/m}^3, \tag{37}$$

where K is expressed in Kelvin.

This section discusses the contact of FGVPs with EFs for the case when the ceramic surface of the FGVPs is in contact with EFs, hence Eqs. (4a) and (5a) are used. The plate parameters are defined as: $\upsilon = 0.6, a = 50h, a/b = 2$, rheological parameter is $\alpha = 0.5$ and the initial conditions are $f_1(0) = f_{10}$ or $f_1'(0) = f_{11}$. In this subsection, the coefficients of the Pasternak elastic foundation are $k_w = 10^7$ (N/m^3) and $k_p = 3.2 \times 10^5$ (N/m). The wave numbers for DS and FV of the FGVPs with and without PEF are $(m, n) = (1, 1)$.

Figures 3, 4, 5 and 6 indicate the time-dependent change of the amplitude function of FG-exponential and FG-inverse quadratic VPs with and without PEF under ICA and ICB, respectively. In Figs. 3, 4, 5 and 6 are

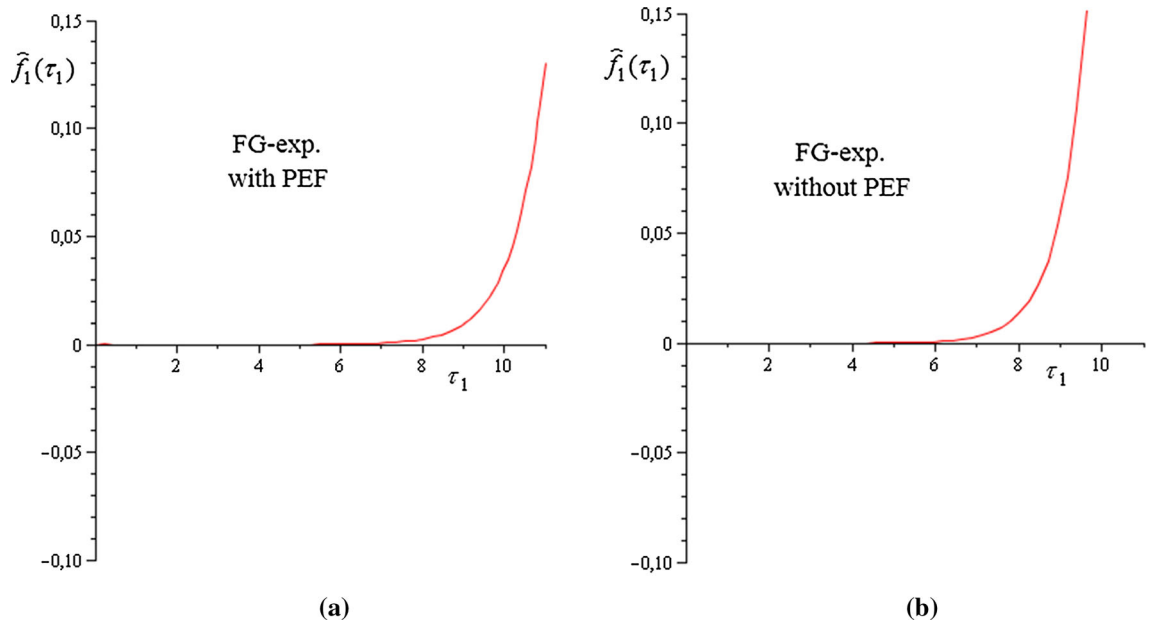

Fig. 4 Change of $f_1^{\frown}(\tau_1)$ for FG-exponential VPs **a** with PEF and **b** without PEF against the τ_1 for the ICB ($f_1(0) = 0,\ f_1'(0) = f_{11}$)

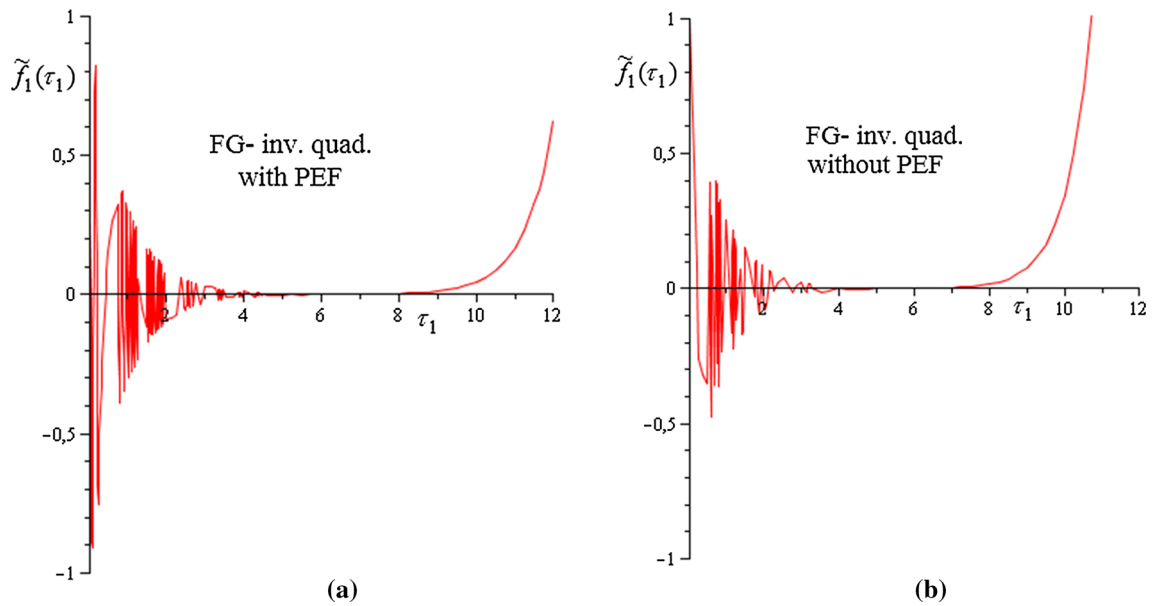

Fig. 5 Change of $\tilde{f}_1(\tau_1)$ for FG-inverse quadratic VPs **a** with PEF and **b** without PEF against the τ_1 for the ICA ($f_1(0) = f_{10},\ f_1'(0) = 0$)

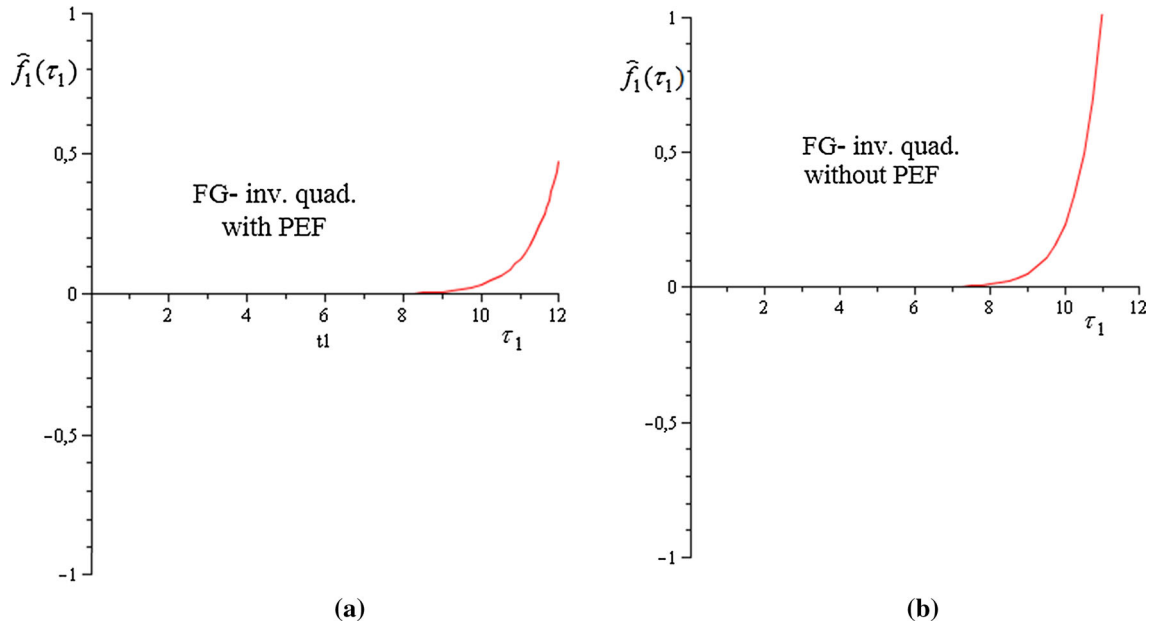

Fig. 6 Change of $\tilde{f}_1(\tau_1)$ for FG-inverse quadratic VPs **a** with PEF and **b** without PEF against the τ_1 for the ICB ($f_1(0) = 0,\ f_1'(0) = f_{11}$)

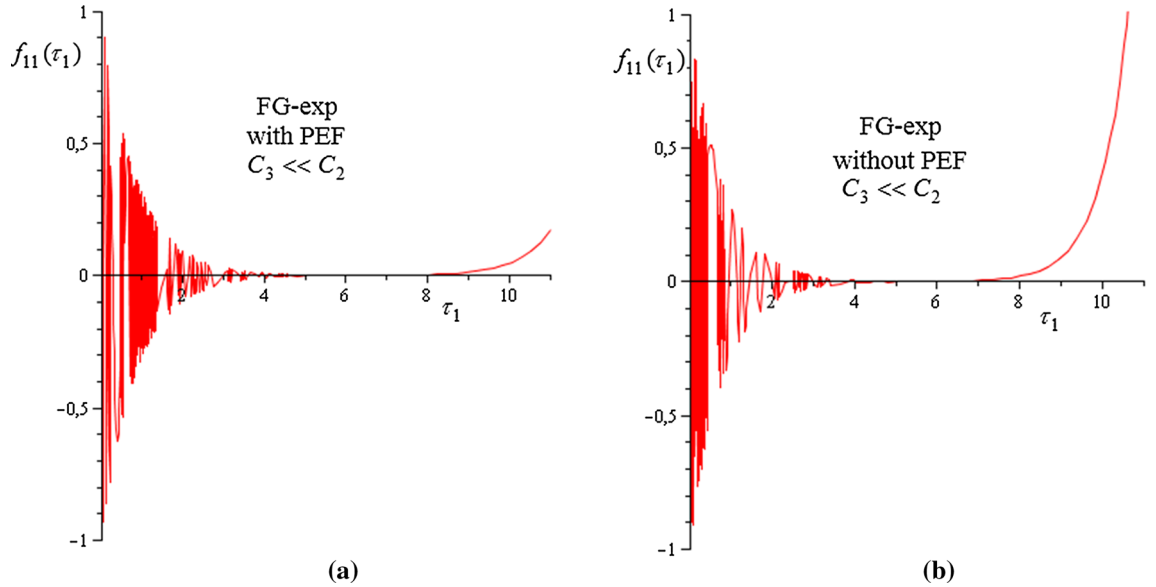

Fig. 7 Change of $f_{11}(\tau_1)$ for FG-exponential VPs **a** with PEF and **b** without PEF for $C_3 << C_2$ against the τ_1 with the ICA ($f_1(0) = f_{10},\ f_1'(0) = 0$)

used: $\tilde{f}_1(\tau_1) = \frac{f_1(\tau_1)}{\tilde{f}_{10}}$ and $f_1^{\frown}(\tau_1) = \frac{f_1(\tau_1)}{\tilde{f}_{11}}$. The wave numbers corresponding to τ_{1cr} for FG-exponential VPs with and without PEF are $(m, n) = (1, 1)$. As seen in Figs. 3, 4, 5 and 6, the time-dependent variation of the amplitude function in FG-exponential and FG-inverse quadratic VPs with and without PEF is characterized by regions having three different characteristics: the region where the amplitude decreases slowly, the transition zone and the region where the amplitude increases suddenly. The beginning of the last zone may be considered as the starting point of the loss of stability. In addition, as shown in Figs. 3, 4, 5 and 6, taking into account the influence of the PEF decreases the rate of increase in the amplitude function of the FGVPs for ICA and ICB.

By using Eqs. (27) and (29), the change of $f_{11}(\tau_1)$ and $f_{12}(\tau_1)$ for FG-exponential VPs with and without PEF versus the τ_1 is indicated in Figs. 7 and 8. The critical time values corresponding to the beginning of the loss of stability of FG-exponential VPs appear to coincide with the values of CTs in Figs. 3 and 4.

Figures 9 and 10 show the change of the amplitude for free vibration of FG-exponential VPs with and without PEF versus τ, by using Eq. (32). Here the following symbols are used: $f_{21}(\tau) = \frac{f_2(\tau)}{f_{10}}$ and $f_{22}(\tau) = \frac{f_2(\tau)}{f_{11}}$. One can see that the presence of viscous resistance leads to damping of the amplitude of FGVPs with and without PEF. From Figs. 9 and 10, it follows that the relaxation rate for FGVPs with and without PEF drops sharply at the beginning of the relaxation processes, and then gradually tends to zero.

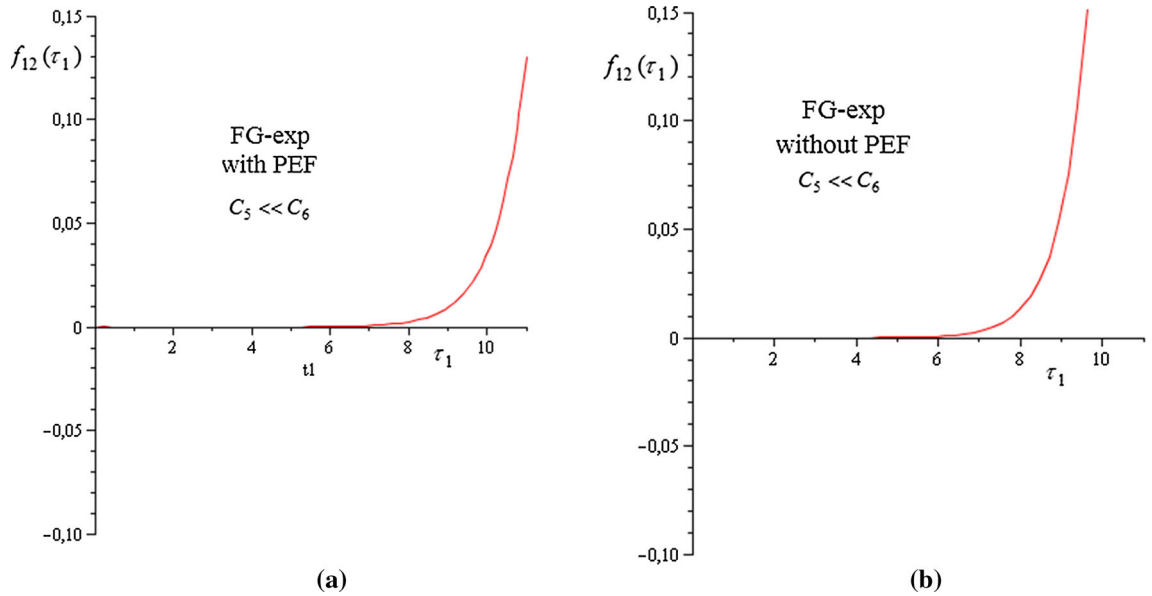

Fig. 8 Change of $f_{12}(\tau_1)$ for FG-exponential VPs **a** with PEF and **b** without PEF for $C_5 << C_6$ against the τ_1 with the ICB ($f_1(0) = 0,\ f_1'(0) = f_{11}$)

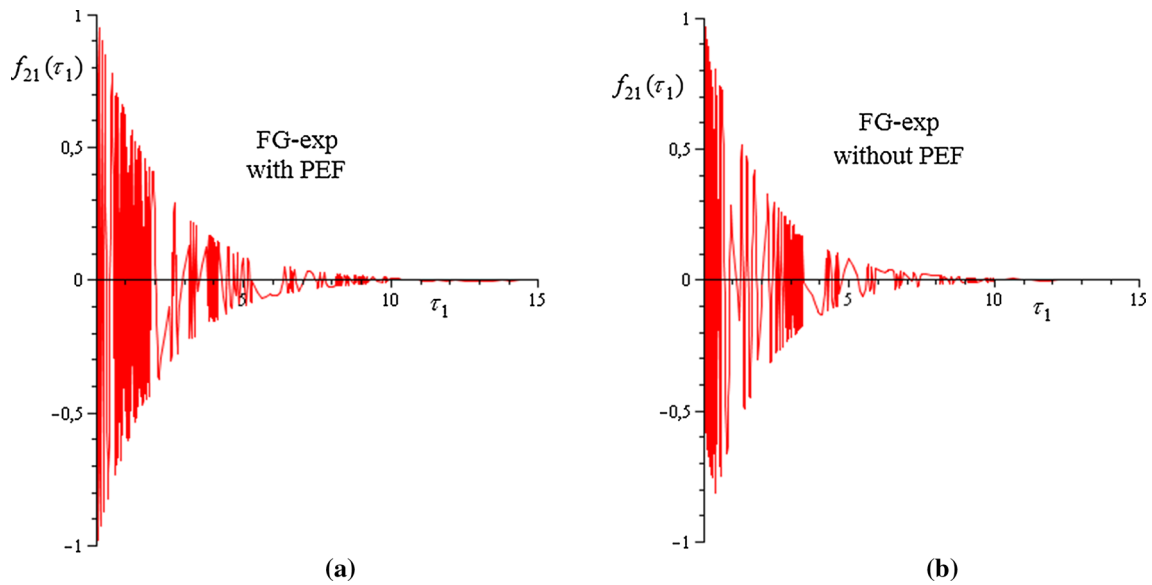

Fig. 9 Change of $f_{21}(\tau_1)$ for the FV of FG-exponential VPs **a** with PEF and **b** without PEF against the τ_1 for the ICA ($f_1(0) = f_{10},\ f_1'(0) = 0$)

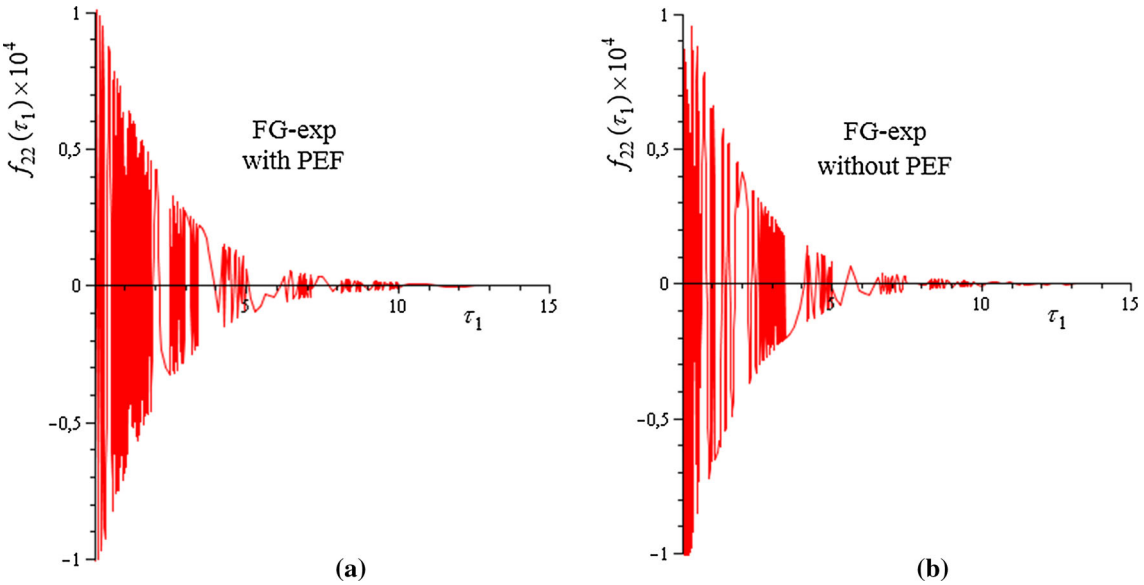

Fig. 10 Change of $f_{22}(\tau_1) \times 10^4$ for the FV of FG-exponential VPs **a** with PEF and **b** without PEF against the τ_1 for the ICB ($f_1(0) = 0,\ f_1'(0) = f_{11}$)

Table 1 Change of CTs for FGVPs, CVP and MVP with and without WEF and PEF versus the loading parameter, υ

	τ_{11wp}^{cr}, ICA					
	SUS304	FG-inv. quad (Eq. 4a)	FG-inv. quad (Eq. 4b)	FG-exp. (Eq. 5a)	FG-exp. (Eq. 5b)	Si_3N_4
υ	$k_w = k_p = 0$					
0.5	8.017	8.459	8.233	8.391	8.391	8.831
0.6	5.454	5.776	5.612	5.727	5.727	6.047
0.7	3.457	3.678	3.565	3.644	3.644	3.864
0.8	1.899	2.035	1.966	2.014	2.014	2.150
υ	$k_w = 3.2 \times 10^7$ (N/m^3), $k_p = 0$					
0.5	8.654	8.978	8.784	8.934	8.934	9.294
0.6	5.847	6.097	5.952	6.062	6.062	6.334
0.7	3.686	3.866	3.764	3.841	3.841	4.033
0.8	2.017	2.133	2.0684	2.116	2.116	2.237
υ	$k_w = 3.2 \times 10^7$ (N/m^3), $k_p = 0.1 \times 10^6$ (N/m)					
0.5	9.065	9.310	9.138	9.281	9.281	9.588
0.6	6.098	6.301	6.168	6.275	6.275	6.515
0.7	3.831	3.890	3.985	3.965	3.965	4.139
0.8	2.091	2.133	2.194	2.180	2.180	2.292
	τ_{12wp}^{cr}, ICB					
υ	$k_w = k_p = 0$					
0.5	3.835	4.056	3.943	4.022	4.022	4.242
0.6	2.601	2.762	2.680	2.737	2.737	2.897
0.7	1.642	1.752	1.696	1.735	1.735	1.845
0.8	0.896	0.964	0.930	0.954	0.954	1.022
υ	$k_w = 3.2 \times 10^7$ (N/m^3), $k_p = 0$					
0.5	4.142	4.307	4.209	4.284	4.284	4.466
0.6	2.790	2.917	2.844	2.899	2.899	3.036
0.7	1.752	1.843	1.792	1.830	1.830	1.927
0.8	0.953	1.011	0.979	1.002	1.002	1.064
υ	$k_w = 3.2 \times 10^7$ (N/m^3), $k_p = 0.1 \times 10^6$ (N/m)					
0.5	4.341	4.467	4.380	4.452	4.452	4.608
0.6	2.911	3.015	2.948	3.002	3.002	3.123
0.7	1.821	1.900	1.852	1.889	1.889	1.978
0.8	0.988	1.040	1.009	1.033	1.033	1.090

Table 2 Change of CTs for FGVPs, CVP and MVP with and without EFs versus the viscoelasticity parameter, α

	τ_{11wp}^{cr}, ICA					
	SUS304	FG-inv. quad (Eq. 4a)	FG-inv. quad (Eq. 4b)	FG-exp. (Eq. 5a)	FG-exp. (Eq. 5b)	Si_3N_4
α	$k_w = k_p = 0$					
0.1	4.262	4.483	4.370	4.449	4.449	4.669
0.3	3.712	3.933	3.821	3.900	3.900	4.120
0.5	3.457	3.678	3.565	3.644	3.644	3.864
0.7	3.289	3.510	3.397	3.476	3.476	3.696
α	$k_w = 4.2 \times 10^7$ (N/m^3), $k_p = 0$					
0.1	4.621	4.775	4.681	4.755	4.755	4.930
0.3	4.033	4.196	4.098	4.174	4.174	4.354
0.5	3.759	3.926	3.828	3.903	3.903	4.086
0.7	3.579	3.749	3.649	3.725	3.725	3.910
α	$k_w = 4.2 \times 10^7$ (N/m^3), $k_p = 10^5$ (N/m)					
0.1	4.795	4.916	4.831	4.902	4.902	5.054
0.3	4.188	4.322	4.232	4.305	4.305	4.466
0.5	3.905	4.045	3.954	4.028	4.028	4.193
0.7	3.719	3.863	3.771	3.845	3.845	4.013
	τ_{12wp}^{cr}, ICB					
α	$k_w = k_p = 0$					
0.1	2.044	2.155	2.098	2.138	2.138	2.248
0.3	1.770	1.880	1.824	1.863	1.863	1.973
0.5	1.642	1.752	1.696	1.735	1.735	1.845
0.7	1.558	1.668	1.612	1.651	1.651	1.761
α	$k_w = 4.2 \times 10^7$ (N/m^3), $k_p = 0$					
0.1	2.218	2.296	2.249	2.286	2.286	2.374
0.3	1.924	2.006	1.957	1.995	1.995	2.086
0.5	1.787	1.872	1.822	1.860	1.860	1.952
0.7	1.697	1.783	1.733	1.771	1.771	1.864
α	$k_w = 4.2 \times 10^7$ (N/m^3), $k_p = 10^5$ (N/m)					
0.1	2.302	2.364	2.321	2.357	2.357	2.434
0.3	1.998	2.067	2.022	2.059	2.059	2.140
0.5	1.857	1.929	1.883	1.920	1.920	2.004
0.7	1.764	1.838	1.791	1.828	1.828	1.914

4.3 New numerical examples for the CTs on the FGVPs resting on the EFs

The numerical examples presented in this subsection for CTs are discussed using the formulas (28) and (30), including various plate characteristics, initial conditions, EF parameters and FGM profiles. The material properties are used by the data specified in the expression (37), and the volume fraction is expressed by inverse quadratic and exponential functions [23–26]. In Tables 1 and 2, the wave numbers are $(m, n) = (1, 1)$.

In Tables 1 and 2, the contact of FGVPs with EFs is discussed for two cases. If the ceramic surface of the FGVPs is in contact with EFs, and Eqs. (4a) and (5a) are used in the calculation, otherwise the metal surface is in contact with EFs, and Eqs. (4b) and (5b) are used. The following data are used in Table 1; $\upsilon = 0.5, 0.6, 0.7, 0.8$, $a/h = 50$, $a/b = 2$, $\alpha = 0.5$, $k_w = 3.2 \times 10^7$ (N/m^3) and $k_p = 10^5$ (N/m). Table 1 shows that the magnitudes of CTs for FGVPs, CVP and MVP with and without EFs decrease with increasing the loading parameter, υ, whereas, the circumferential wave numbers corresponding to CTs remain constant for (a) ICA and (b) ICB. The magnitudes of CTs for FGVPs, CVP and MVP with and without EFs for ICB are notably lower than for the ICA. Comparing the FGVPs on the WEF with the unconstrained FGVPs, the influences of WEF and PEF on the magnitudes of CTs decrease with increasing loading parameter, υ, while the influence of the PEF is higher than the WEF effect for ICA and ICB. Comparing the FGVPs with the MVP (or the CVP), taking into account the effect of WEF and PEF, the effects of FGMs on the CTs increase, whereas for the case of PEF, the FGM profiles have little effect and it slightly increases with increasing loading parameter υ. In addition, the influences of FGMs on the CTs for FGVPs with EF_S are lower than the effect of FGMs in unconstrained FGVPs for ICA and ICB. Since CTs for both exponential changes take the same value, it does not matter which side of the FGVPs is in contact with the EFs. For the FG-inverse quadratic profile, when the metal surface of the FGVPs is at the top, it is seen that the critical time values are greater than the case when the metal surface is lower (with or without EFs) and this difference decreases as υ increases.

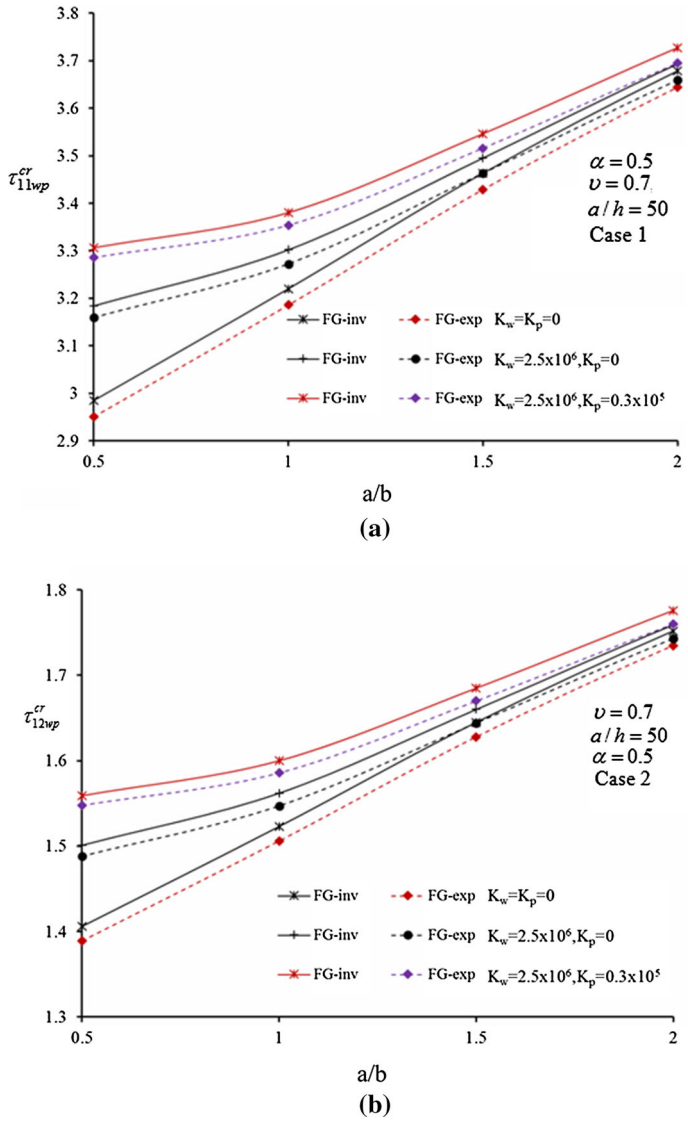

Fig. 11 Change of CTs for FGVPs, CVP and MVP with and without EFs for **a** ICA and **b** ICB, versus the a/b

The change of CTs for FVFP CVP and MVP with and without EFs depending on the ratio a/b, the plate parameters and EF coefficients is indicated in Fig. 11 for (a) ICA and (b) ICB. For Fig. 11, the expressions (4a) and (5a) are used. From Fig. 11, we can conclude that the magnitudes of CTs for FGVPs, CVP and MVP with and without EFs for (a) ICA and (b) ICB increase as the ratio a/b increases. While the influences of WEF and PEF on the CTs are significantly reduced, the effects of FGMs on the CTs are slightly reduced with an increase of a/b for ICA and ICB. In both initial conditions, the PEF effect on the CTs is more pronounced than the WEF effect, as a/b changes. The effect of the FGM-inverse quadratic profile on the CTs for FGVPs, CVP and MVP with and without EFs is more pronounced than the effect of the FGM-exponential profile.

The values of τ_{11wp}^{cr} and τ_{12wp}^{cr} for FGVPs, CVP and MVP with and without WEF and PEF depending on the viscoelasticity parameter α are calculated and tabulated in Table 2. Here, the following data are used: $a/h = 50$, $a/b = 2$, $k_w = 4.2 \times 10^7$ (N/m^3), $k_p = 10^5$ (N/m) and $\upsilon = 0.7$. As shown in Table 2, the values of CTs continuously decrease, while the number of circumferential waves remains constant, with increasing α. While the influences of ground and FGMs are increasing with increasing viscoelastic parameter α, the influences of FGMs on the CTs of FGVPs resting on the EFs decrease, as compared to unconstrained FGVPs. Although the values of CTs for the ICA are significantly higher than for the ICB, the influences of FGMs or EFs are about the same as the percentages. From Table 2, it can be seen that when Eqs. (4a) are used, the

critical time values are higher than with Eqs. (4b) are used (with or without EFs) for the FG-inverse quadratic profile, and this difference does not depend on α.

5 Conclusions

The free vibration and dynamic stability analysis of FGVPs on Winkler and Pasternak elastic foundations under compressive load in the x direction for ICA and ICB are examined. The concepts of Boltzmann and Volterra are used to derive the basic equations of FGVPs on EFs. The Galerkin and the Laplace method are used to solve the current problem. The expressions for amplitudes and CTs for FGVPs on EFs are obtained. The obtained results are proved by comparing them with other existing solutions. Finally, the influences of EFs, FGMs, loading parameters and viscoelasticity parameter on the CTs have been investigated in detail.

Appendix A

$$
\begin{aligned}
L_{11} &= hu_2\frac{\partial^4}{\partial x_1^4} + 2h\left(u_1 - u_5\right)\frac{\partial^4}{\partial x_1^2\partial x_2^2} + hu_2\frac{\partial^4}{\partial x_2^4},\\
L_{12} &= -u_3\frac{\partial^4}{\partial x_1^4} - \left(u_4 + 2u_6 + u_3\right)\frac{\partial^4}{\partial x_1^2\partial x_2^2} - u_4\frac{\partial^4}{\partial x_2^4},\\
L_{13} &= -\mathrm{P}\frac{\partial^2}{\partial x_1^2} - k_w + k_p\left(\frac{\partial^2}{\partial x_1^2} + \frac{\partial^2}{\partial x_2^2}\right) - \bar{\rho}_f\frac{\partial^2}{\partial \tau^2},\\
L_{21} &= hv_1\frac{\partial^4}{\partial x_1^4} + h\left(2v_2 + v_5\right)\frac{\partial^4}{\partial x_1^2\partial x_2^2} + hv_1\frac{\partial^4}{\partial x_2^4},\\
L_{22} &= -v_4\frac{\partial^4}{\partial x_1^4} - \left(2v_3 - v_6\right)\frac{\partial^4}{\partial x_1^2\partial x_2^2} - v_4\frac{\partial^4}{\partial x_2^4},
\end{aligned}
\tag{A1}
$$

where

$$
\begin{aligned}
&u_1 = w_1^1 v + w_2^1 v_2, \quad u_2 = w_1^1 v_2 + w_2^1 v_1, \quad u_3 = w_1^1 v_3 + w_2^1 v_4 + w_1^2, \quad u_4 = w_1^1 v_4 + w_2^1 v_3 + w_2^2,\\
&u_5 = w_6^1 v_5, \quad u_6 = w_6^1 v_6 + 2w_6^2, \quad v_1 = \frac{w_1^0}{\Pi}, \quad v_2 = -\frac{w_2^0}{\Pi}, \quad v_3 = \frac{w_2^0 w_1^1 - w_1^1 w_1^0}{\Pi},\\
&v_4 = \frac{w_2^0 w_1^1 - w_2^1 w_1^0}{\Pi}, \quad v_5 = \frac{1}{w_6^0}, \quad v_6 = -\frac{2w_6^1}{w_6^0}, \quad \Pi = w_1^0 w_1^0 - w_2^0 w_2^0,
\end{aligned}
\tag{A2}
$$

in which

$$
w_1^k = \int_{-h/2}^{h/2} \frac{E_f}{1-\nu_f^2} x_3^k \mathrm{d}x_3, \quad w_2^k = \int_{-h/2}^{h/2} \frac{\nu_f E_f}{1-\nu_f^2} x_3^k \mathrm{d}x_3, \quad w_6^k = \int_{-h/2}^{h/2} \frac{E_f}{2\left(1+\nu_f\right)} x_3^k \mathrm{d}x_3, \quad k = 0, 1, 2. \tag{A3}
$$

References

1. Bland, D.R.: The Theory of Linear Viscoelasticity. Pergamon Press, Oxford (1960)
2. Christensen, R.M.: Theory of Viscoelasticity. Dover, New York (1982)
3. Il'yushin, A., Pobedrya, B.: Foundations of Mathematical Theory of Thermoviscoelasticity. Nauka, Moscow (1970)
4. Ogibalov, P., Lomakin, V., Kishkin, B.: Mechanics of Polymers. Moscow State University, Moscow (1975)
5. Aboudi, J., Cederbaum, G., Elishakoff, I.: Dynamic stability analysis of viscoelastic plates by Lyapunov exponents. J. Sound Vib. **139**(3), 459–467 (1990). https://doi.org/10.1016/0022-460X(90)90676-Q
6. Badalov, F., Eshmatov, K., Akbarov, U.: Stability of a viscoelastic plate under dynamic loading. Sov. Appl. Mech. **27**(9), 892–899 (1991). https://doi.org/10.1007/BF00887982
7. Hui, D.: Viscoelastic response of floating ice plates under distributed or concentrated loads. J. Strain Anal. Eng. Design **21**(3), 135–143 (1986). https://doi.org/10.1243/03093247V213135

8. Pan, H.: Vibrations of viscoelastic plates. Journal de Mécanique **5**, 355–374 (1966)
9. Aköz, A.Y., Kadıoğlu, F., Tekin, G.: Quasi-static and dynamic analysis of viscoelastic plates. Mech. Time Depend. Mater. **19**(4), 483–503 (2015). https://doi.org/10.1007/s11043-015-9274-8
10. Alibeigloo, A.: Effect of viscoelastic interface on three-dimensional static and vibration behavior of laminated composite plate. Compos. Part B Eng. **75**, 17–28 (2015). https://doi.org/10.1016/j.compositesb.2015.01.025
11. Arruda, M., Garrido, M., Castro, L., Ferreira, A., Correia, J.: Numerical modelling of the creep behaviour of GFRP sandwich panels using the Carrera Unified Formulation and Composite Creep Modelling. Compos. Struct. **183**, 103–113 (2018). https://doi.org/10.1016/j.compstruct.2017.01.074
12. Ferreira, A., Araújo, A., Neves, A., Rodrigues, J., Carrera, E., Cinefra, M., Soares, C.M.: A finite element model using a unified formulation for the analysis of viscoelastic sandwich laminates. Compos. Part B Eng. **45**(1), 1258–1264 (2013). https://doi.org/10.1016/j.compositesb.2012.05.012
13. Ilyasov, M.: Dynamic stability of viscoelastic plates. Int. J. Eng. Sci. **45**(1), 111–122 (2007). https://doi.org/10.1016/j.ijengsci.2006.08.016
14. Ilyasov, M., Aköz, A.: The vibration and dynamic stability of viscoelastic plates. Int. J. Eng. Sci. **38**(6), 695–714 (2000). https://doi.org/10.1016/S0020-7225(99)00060-9
15. Luis, N.F., Madeira, J.F.A., Araújo, A., Ferreira, A.: Active vibration attenuation in viscoelastic laminated composite panels using multiobjective optimization. Compos. Part B Eng. **128**, 53–66 (2017). https://doi.org/10.1016/j.compositesb.2017.07.002
16. Tang, Y.-Q., Chen, L.-Q.: Parametric and internal resonances of in-plane accelerating viscoelastic plates. Acta Mech. **223**(2), 415–431 (2012). https://doi.org/10.1007/s00707-011-0567-y
17. Tekin, G., Kadıoğlu, F.: Viscoelastic behavior of shear-deformable plates. Int. J. Appl. Mech. **9**(6), 1750085 (2017). https://doi.org/10.1142/S1758825117500855
18. Zenkour, A.: Buckling of fiber-reinforced viscoelastic composite plates using various plate theories. J. Eng. Math. **50**(1), 75–93 (2004). https://doi.org/10.1023/B:ENGI.0000042123.94111.35
19. Zhou, X., Yu, D., Shao, X., Zhang, S., Wang, S.: Research and applications of viscoelastic vibration damping materials: a review. Compos. Struct. **136**, 460–480 (2016). https://doi.org/10.1016/j.compstruct.2015.10.014
20. Ostoja-Starzewski, M., Jasiuk, I., Wang, W., Alzebdeh, K.: Composites with functionally graded interfaces: meso-continuum concept and effective properties. Acta Mater. **44**(5), 2057–2066 (1996). https://doi.org/10.1016/1359-6454(95)00269-3
21. Kieback, B., Neubrand, A., Riedel, H.: Processing techniques for functionally graded materials. Mater. Sci. Eng. A **362**(1–2), 81–106 (2003). https://doi.org/10.1016/S0921-5093(03)00578-1
22. Shen, H.-S.: Functionally Graded Materials: Nonlinear Analysis of Plates and Shells. CRC Press, Florida (2009)
23. Saharan, A., Ostoja-Starzewski, M., Koric, S.: Fractal geometric characterization of functionally graded materials. ASCE J. Nanomech. Micromech. **3**(4), 04013001-1-13 (2013). https://doi.org/10.1061/(ASCE)NM.2153-5477.0000058
24. Sofiyev, A., Zerin, Z., Kuruoglu, N.: Thermoelastic buckling of FGM conical shells under non-linear temperature rise in the framework of the shear deformation theory. Compos. Part B Eng. **108**, 279–290 (2017). https://doi.org/10.1016/j.compositesb.2016.09.102
25. Tornabene, F., Fantuzzi, N., Bacciocchi, M.: Free vibrations of free-form doubly-curved shells made of functionally graded materials using higher-order equivalent single layer theories. Compos. Part B Eng. **67**, 490–509 (2014). https://doi.org/10.1016/j.compositesb.2014.08.012
26. Tornabene, F., Fantuzzi, N., Viola, E., Batra, R.C.: Stress and strain recovery for functionally graded free-form and doubly-curved sandwich shells using higher-order equivalent single layer theory. Compos. Struct. **119**, 67–89 (2015). https://doi.org/10.1016/j.compstruct.2014.08.005
27. Pitakthapanaphong, S., Busso, E.: Self-consistent elastoplastic stress solutions for functionally graded material systems subjected to thermal transients. J. Mech. Phys. Solids **50**(4), 695–716 (2002). https://doi.org/10.1016/S0022-5096(01)00105-3
28. Jin, Z.H., Batra, R.C.: Stress intensity relaxation at the tip of an edge crack in a functionally graded material subjected to a thermal shock. J. Therm. Stress. **19**, 317–339 (1996). https://doi.org/10.1080/01495739608946178
29. Zenkour, A.: Benchmark trigonometric and 3-D elasticity solutions for an exponentially graded thick rectangular plate. Arch. Appl. Mech. **77**(4), 197–214 (2007). https://doi.org/10.1007/s00419-006-0084-y
30. Ashrafi, H., Shariyat, M., Khalili, S., Asemi, K.: A boundary element formulation for the heterogeneous functionally graded viscoelastic structures. Appl. Math. Comput. **225**, 246–262 (2013). https://doi.org/10.1016/j.amc.2013.09.025
31. Jin, Z.: Some notes on the linear viscoelasticity of functionally graded materials. Math. Mech. Solids **11**(2), 216–224 (2006). https://doi.org/10.1177/1081286504040401
32. Khan, K.A., Muliana, A.H.: A multi-scale model for coupled heat conduction and deformations of viscoelastic functionally graded materials. Compos. Part B Eng. **40**(6), 511–521 (2009). https://doi.org/10.1016/j.compositesb.2009.02.003
33. Mukherjee, S., Paulino, G.H.: The elastic–viscoelastic correspondence principle for functionally graded materials, revisited. J. Appl. Mech. **70**(3), 359–363 (2003). https://doi.org/10.1115/1.1533805
34. Mao, Y., Fu, Y., Dai, H.: Creep buckling and post-buckling analysis of the laminated piezoelectric viscoelastic functionally graded plates. Eur. J. Mech. A Solids **30**(4), 547–558 (2011). https://doi.org/10.1016/j.euromechsol.2011.03.004
35. Zenkour, A.: Viscoelastic analysis of an exponentially graded sandwich plate. J. Mech. Sci. Technol. **26**(3), 889–898 (2012). https://doi.org/10.1007/s12206-011-1244-8
36. Shariyat, M., Nasab, F.F.: Low-velocity impact analysis of the hierarchical viscoelastic FGM plates, using an explicit shear-bending decomposition theory and the new DQ method. Compos. Struct. **113**, 63–73 (2014). https://doi.org/10.1016/j.compstruct.2014.03.003
37. Barretta, R., Feo, L., Luciano, R.: Torsion of functionally graded nonlocal viscoelastic circular nanobeams. Compos. Part B Eng. **72**, 217–222 (2015). https://doi.org/10.1016/j.compositesb.2014.12.018
38. Yang, C., Jin, G., Ye, X., Liu, Z.: A modified Fourier–Ritz solution for vibration and damping analysis of sandwich plates with viscoelastic and functionally graded materials. Int. J. Mech. Sci. **106**, 1–18 (2016). https://doi.org/10.1016/j.ijmecsci.2015.11.031

39. Deng, J., Liu, Y., Zhang, Z., Liu, W.: Stability analysis of multi-span viscoelastic functionally graded material pipes conveying fluid using a hybrid method. Eur. J. Mech. A Solids **65**, 257–270 (2017). https://doi.org/10.1016/j.euromechsol.2017.04.003
40. Li, C., Liu, J., Cheng, M., Fan, X.: Nonlocal vibrations and stabilities in parametric resonance of axially moving viscoelastic piezoelectric nanoplate subjected to thermo-electro-mechanical forces. Compos. Part B Eng. **116**, 153–169 (2017). https://doi.org/10.1016/j.compositesb.2017.01.071
41. Sofiyev, A.: On the solution of the dynamic stability of heterogeneous orthotropic visco-elastic cylindrical shells. Compos. Struct. **206**, 124–130 (2018). https://doi.org/10.1016/j.compstruct.2018.08.027
42. Sofiyev, A.: About an approach to the determination of the critical time of viscoelastic functionally graded cylindrical shells. Compos. Part B Eng. **156**, 156–165 (2019). https://doi.org/10.1016/j.compositesb.2018.08.073
43. Kerr, A.D.: Elastic and viscoelastic foundation models. J. Appl. Mech. **31**(3), 491–498 (1964). https://doi.org/10.1115/1.3629667
44. Pasternak, P.L.: On a new method of analysis of an elastic foundation by means of two foundation constants. Gosudarstvennoe Izdatelstvo Literaturi po Stroitelstvu i Arkhitekture, Moscow (1954)
45. Vlasov, V.Z., Leont'ev, N.: Beams, plates and shells on elastic foundation. Israel Program for Scientific Translation, Jemsalem (1966)
46. Zenkour, A., Sobhy, M.: Elastic foundation analysis of uniformly loaded functionally graded viscoelastic sandwich plates. J. Mech. **28**(3), 439–452 (2012). https://doi.org/10.1017/jmech.2012.53
47. Zenkour, A.M., Allam, M., Sobhy, M.: Bending analysis of FG viscoelastic sandwich beams with elastic cores resting on Pasternak's elastic foundations. Acta Mech. **212**(3–4), 233–252 (2010). https://doi.org/10.1007/s00707-009-0252-6
48. Shariyat, M., Alipour, M.: A power series solution for vibration and complex modal stress analyses of variable thickness viscoelastic two-directional FGM circular plates on elastic foundations. Appl. Math. Model. **37**(5), 3063–3076 (2013). https://doi.org/10.1016/j.apm.2012.07.037
49. Hosseini, S.M., Kalhori, H., Shooshtari, A., Mahmoodi, S.N.: Analytical solution for nonlinear forced response of a viscoelastic piezoelectric cantilever beam resting on a nonlinear elastic foundation to an external harmonic excitation. Compos. Part B Eng. **67**, 464–471 (2014). https://doi.org/10.1016/j.compositesb.2014.08.015
50. Sobhy, M., Zenkour, A.M.: Magnetic field effect on thermomechanical buckling and vibration of viscoelastic sandwich nanobeams with CNT reinforced face sheets on a viscoelastic substrate. Compos. Part B Eng. **154**, 492–506 (2018). https://doi.org/10.1016/j.compositesb.2018.09.011
51. Liu, H., Liu, H., Yang, J.: Vibration of FG magneto-electro-viscoelastic porous nanobeams on visco-Pasternak foundation. Compos. Part B Eng. **155**, 244–256 (2018). https://doi.org/10.1016/j.compositesb.2018.08.042
52. Deniz, A., Zerin, Z., Karaca, Z.: Winkler-Pasternak foundation effect on the frequency parameter of FGM truncated conical shells in the framework of shear deformation theory. Compos. Part B Eng. **104**, 57–70 (2016). https://doi.org/10.1016/j.compositesb.2016.08.006
53. Haciyev, V., Sofiyev, A., Kuruoglu, N.: On the free vibration of orthotropic and inhomogeneous with spatial coordinates plates resting on the inhomogeneous viscoelastic foundation. Mech. Adv. Mater. Struct., 1–12 (2018). https://doi.org/10.1080/15376494.2018.1430271
54. Matyash, V.: Parametric oscillations of a viscoelastic cylindrical shell. Polym. Mech. **10**(3), 402–405 (1974). https://doi.org/10.1007/BF00865596